Cinematographic study of stochastic chemical events at atomic resolution
Running Title: Sub-millisecond single-molecule TEM imaging

Koji Harano*, Takayuki Nakamuro and Eiichi Nakamura*

Authors:
Koji Harano
Center for Basic Research on Materials, National Institute for Materials Science, 1-1 Namiki, Tsukuba, Ibaraki, 305-0044, Japan
harano.koji@nims.go.jp
TEL: +81-29-860-4965

Takayuki Nakamuro
Department of Chemistry, The University of Tokyo, 7-3-1 Hongo, Bunkyo-ku, Tokyo, 113-0033, Japan
muro@chem.s.u-tokyo.ac.jp
TEL: +81-3-5841-4369

Eiichi Nakamura
Department of Chemistry, The University of Tokyo, 7-3-1 Hongo, Bunkyo-ku, Tokyo, 113-0033, Japan
nakamura@chem.s.u-tokyo.ac.jp
TEL: +81-3-5841-4356

Corresponding authors:
Koji Harano and Eiichi Nakamura

Keywords:
SMART-EM, in situ imaging, direct electron detection camera, image processing, chemical reaction, molecular motion

Manuscript Information:
46 pages, and 12 figures in total.

Mini-Abstract (50 word maximum)

This review showcases the development of dynamic molecular imaging using the single-molecule atomic-resolution time-resolved electron microscopy (SMART-EM) technique, highlighting the tracking of stochastic molecular motions and chemical reactions with sub-millisecond temporal resolution and sub-angstrom localization precision, supported by the development of fast CMOS cameras and denoising techniques.

The figure that best represents this paper: Figure 5

Abstract

The advent of single-molecule atomic-resolution time-resolved electron microscopy (SMART-EM) has created a new field of "cinematic chemistry," allowing for the cinematographic recording of dynamic behaviors of organic and inorganic molecules and their assembly. However, the limited electron dose per frame of video images presents a major challenge in SMART-EM. Recent advances in direct electron counting cameras and techniques to enhance image quality through the implementation of a denoising algorithm have enabled the tracking of stochastic molecular motions and chemical reactions with sub-millisecond temporal resolution and sub-angstrom localization precision. This review showcases the development of dynamic molecular imaging using the SMART-EM technique, highlighting insights into nanomechanical behavior during molecular shuttle motion, pathways of multistep chemical reactions, and elucidation of crystallization processes at the atomic level.

Introduction

In the 19th century, Eadweard Muybridge achieved a significant breakthrough by using multiple cameras to capture continuous photographs of a galloping horse. Through his work, Muybridge became the first to demonstrate that all four legs of a horse leave the ground at a certain moment during the gallop [1]. In recent years, advancements in slow-motion photography and high-speed cameras have allowed us to witness the mesmerizing phenomenon of "milk crown" formation. This nearly instantaneous process occurs when a droplet of milk is released onto a liquid surface, resulting in the creation of a beautiful crown-shaped pattern. Thus, the use of fast cameras has an artistic appeal in capturing the fleeting beauty of nature and serves as a crucial research technique, providing direct

evidence of various chemical phenomena and physical laws.

In the field of materials science, scientists have long aspired to observe the motions of individual molecules at the atomic level. However, achieving both spatial resolution for visualizing atoms and molecules and temporal resolution for tracking their high-speed motions, structural changes, and reactions, has posed a challenge. An often-overlooked problem here is the intrinsic stochasticity of the molecular event. We may find only one molecular event of microsecond duration during observation of an area of tens of nm^2 for 10 min, and we need to study tens of them to ensure statistical accuracy—a formidable challenge for any microscopic or spectroscopic technologies.

Two challenging issues in the TEM imaging of organic molecules in motion have therefore been recognized. The first is the structural flexibility and the motions, and the second is the very weak image contrast of molecules that largely consist of the first and the second row elements. One way to resolve these problems reported in the 1970s was to freeze the molecules in crystals, acquiring superimposed images of rigid aromatic organic molecules in a crystal [2,3]. A recent strategy along this venue utilizes a crystalline zeolite as a substrate to trap molecules in its cavity [4]. However, this strategy cannot be used for dynamic molecular imaging, as is the cryo-EM method. The liquid-cell TEM method allows us only to image heavy elements and their assemblies (e.g., metal nanoparticles), but not single organic molecules, whose images are drowned out by the background noise of the solvent and the liquid-cell membranes [5].

Atomic force microscopy (AFM) have made remarkable progress in tracking the motions

of biomolecules, enabling the capture of several tens of frames per second (fps), the resolution is limited because of the nature of the scanning principle [6,7]. AFM at the highest speed regime is limited in spatial resolution, making it impossible to observe atomic-level structures. In addition, AFM can deal with objects fixed on a macroscopic substrate, a common limitation of scanning probe microscopy.

Today, electron microscopy has become a widely used analytical tool in materials science and biology. Its application to chemical research, particularly in molecular science, has rapidly expanded in recent years [8]. Mechanical motions and chemical reactions at the single-molecule level, which are intricately influenced by quantum control and environmental fluctuations, have garnered interest in chemistry, physics, and nanoscience. Because of advancements such as aberration-corrected TEM, which allows the observation of atomistic structures at the angstrom level, direct electron detection cameras capable of high-speed imaging with low background noise, and various image-collection and processing software, the longstanding dream of "observing molecular motions and reactions as atomic-resolution images" is now becoming a reality. Notably, numerous impactful images have been reported in recent years, leaving a profound impact on research and education. While the 20th century was the "era of cinema", the 21st century has opened the doors to the realm of cinematic chemistry, marking a new era for chemical science.

In this review, we focus on millisecond-scale single-molecule atomic-resolution time-resolved electron microscopy (SMART-EM) imaging as an example of research in cinematic chemistry. We explore its application in directly observing molecular dynamics,

including molecular motion, chemical reactions, molecular translocation, shuttle motion imaging, and the observation of salt crystal formation processes (nucleation and crystal growth) using high-speed electron microscopes and image noise reduction protocols. Our aim is to provide examples of high-speed TEM imaging and to discuss how atomic-resolution high-speed imaging has brought about a new understanding of atomic and molecular phenomena encountered in molecular and nanoscience. SMART-EM will be the key technology for transforming chemistry from thermodynamics-based to statistical mechanics-based science.

Single-molecule atomic-resolution time-resolved electron microscopy (SMART-EM)

A pioneering field of molecular science is unfolding. This area uses high-resolution, time-resolved TEM to capture real-time images of the behaviors of molecules and their assemblies that lack periodic structures. This research using SMART-EM aims to bridge the gap between chemistry and electron microscopy. SMART-EM provides a unique way to observe dynamic changes in molecules, such as structural transformations or chemical reactions, at an atomic level and in real time. For instance, it can capture conformational shifts and assembly processes either with or without chemical bond recombination.

In 2004, one of the authors (E.N.) challenged the long-held belief in electron microscopy that "organic and inorganic molecules disintegrate immediately under electron microscopic observation" and started an Exploratory Research for Advanced Technology project sponsored by Japan Agency for Science and Technology. The group demonstrated that it is possible to observe structural changes in molecules loosely contained within and outside single-walled carbon nanotubes (CNTs) [9]. Fig. 1 displays a series of TEM video

frames showing two hydrocarbon chains attached to carborane, changing their structure every second. Carborane is a boron-carbon cluster used as a TEM marker. Although the original 2007 TEM video's temporal and spatial resolution was very low from the present-day perspective (2.1 sec per frame and ca 2 Å spatial resolution), this experiment was a landmark. It showed for the first time that it is feasible to observe, in real time, changes in the structure of a single hydrocarbon molecule without decomposition, paving the way for using electron microscopy to study the dynamic behavior of molecules. Indeed, since our report in 2007, many researchers have published papers on atomic-resolution TEM video imaging of organic and inorganic molecules [10,11,12,13,14,15,16]. After decade-long cinematographic studies of chemical events at atomic resolution, we have recently stepped into a new paradigm of chemical analysis – statistical studies on the kinetics and thermodynamics of stochastic behavior of atoms and molecules. Some of such data we obtained were found to match well with the data obtained by conventional ensemble-average and thermodynamic measurements [17,18,19] (Fig, 2).

Scattering of electrons by atoms involves two basic mechanisms, elastic and inelastic scattering. The elastic collision results in atom displacement (so called knock-on), though the cross section is extremely small for light elements. As pointed out by Egerton [20], this pathway negligibly affects the imaging of organic molecules, corroborating well with our experience in the SMART-EM experiments. On the other hand, inelastic scattering occurs far more frequently, triggering a variety of processes, among which vibrational excitation, electronic excitation, and ionization (radiolysis) are particularly important in the chemistry of electron microscopy. The energy required for vibrational excitation is extremely low, ranging from 0.1 to 0.4 eV, occurring first among other events in a

picosecond timeframe [21]. In contrast, the bond dissociation energy induced by electronic excitation or ionization is around several eV, making it a considerably less likely chemical process occurring in a nano to microsecond timeframe. Our recent studies suggest that the grounding effects exerted by conductive CNT and graphene substrate further contributes to the stability of organic molecule under electron irradiation [19].

Most of the SMART-EM study has been performed with an acceleration voltage higher than 60 kV where we can stably obtain high-resolution images and lower than 120 kV where CNT support remained stable. At temperatures as low at 100 K, CNT and graphene lose structural integrity (e.g., π-network) [22], and we used temperatures between 300 K and 1000 K in most of the SMART-EM studies.

The use of CNTs as a sample carrier for observing molecules enabled the visualization of single-molecule dynamics by SMART-EM. However, to transform this technique into a problem-solving tool for science and society, we need innovations in TEM and related equipment. The Japanese Society of Microscopy has recently introduced the concept of electron microscopy 5.0 (EM 5.0) [23], emphasizing the necessity of integrating electron microscope hardware and software, often developed separately. The future of SMART-EM aligns with this proposal: advanced electron gun development will enhance single-atom and molecule contrast by achieving high-resolution observation at low acceleration voltages.

The SMART-EM imaging requires an electron dose rate (EDR) of 10^5 to 10^6 e^{-1} nm^{-2}, 100 to 1000 times larger than the one used for electron diffraction and microscopic studies

of crystals and solids. It is simply because the single molecule specimens are held in a vacuum, and most of the electrons pass through the vacuum and have no interaction with the specimen. Historically the word "dose" originated from the amount of pharmaceuticals administered to the human body, and is used as a standard for evaluating the effects of X-ray irradiation on the human body. In the field of electron microscopy, this term assumes that most of the electrons irradiated from the electron gun are absorbed by a thick TEM sample, which is not the case in SMART-EM imaging. SMART-EM imaging using CNT or graphene as a substrate in a vacuum therefore provides images of much higher contrast and resolution for molecules than the liquid-cell and cryo-EM imaging.

Further, the creation of ultra-sensitive cameras and detectors will lead to improved image quality. Supporting these hardware advancements requires software capable of automatic processing of data generated by ultrafast cameras and automatic correction and observation. While advancements in aberration-corrected electron microscopes, direct electron detection (DED) cameras, and noise reduction algorithms now allow routine imaging of atoms and molecules at high temporal and spatial resolutions of sub-milliseconds and 1 Å, further technological development remains essential.

Real-time observation of irreversible events by TEM

Electron microscopy combined with the high-speed pump-and-probe technique has been developed for the observation of rapid events in real time. Often referred to as 4D-EM, this method uses a pulsed light, or pump light, to excite the specimen and a probe electron beam to track the resulting structural changes [24,25]. Time-resolved electron diffraction,

another technique, also uses a pulsed electron beam to observe transient structural changes in the excited state of solids with femtosecond time resolution [26]. However, these techniques require precise timing of pump light application, making them unamenable to the study of stochastic, chaotic, and irreversible chemical phenomena.

Notably, the ability of SMART-EM to continuously image chemical events in situ excels in tracking stochastic molecular dynamics. It allows us to study individual molecules and to statistically analyze the chemistry. The timescale of the observation ranges from milliseconds to tens of minutes and is suitable for tracking chemical reactions whose time scale ranges from microseconds to hours. The time scale of the pump-probe methods is too short to follow the whole reaction course of many molecules.

Cinematographic imaging is a powerful tool for understanding the complex dynamic behaviors of individual molecules. However, imaging at a millisecond scale for tens of minutes generates an enormous amount of image data. Therefore, the application of data science methods, such as signal-to-noise ratio improvement and automatic detection by AI, is crucial to identify chemically significant events out of the mass of images.

The advancement in imaging devices, starting from photosensitive films to charge-coupled devices (CCDs) and complementary metal oxide semiconductors (CMOSs), has catalyzed the development of high-precision, high-speed electron microscope cameras. The fast cameras contributed to the development of the cryo-EM technique culminating in a recent Nobel Prize in Chemistry [27]. The success sparked interest in high-speed moving image imaging of molecules. In 2008, an early instance of using a high-speed

CCD camera allowed imaging to be recorded at a rate of 12 fps [28].

Sub-millisecond high-speed video capture using a DED camera

In response to the need for faster cameras to help reveal fast-paced atomic and ionic phenomena, a high-speed K2-IS camera, capable of capturing images at 400 fps for full frame and up to 1600 fps in restricted pixel size, was introduced in 2014 by Gatan (now Ametek). With this camera, Liao, Zheng, and colleagues reported on in situ recordings of atomic layer growth on a platinum crystal surface at a speed of 80 fps in liquid-cell TEM observations using an average of five frames from raw 400 fps data [29].

This new high-speed imaging device has proven especially effective in directly visualizing the dynamics of metal particle surfaces composed of heavy atoms [30] successfully recording real-time videos of catalyst particle dynamics [31], and CNT growth processes [32]. However, for high-speed imaging of atomically thin samples, the signal-to-noise ratio (SNR) of a single frame of an unprocessed original video is often insufficient. In most cases, the SNR needs to be enhanced by overlapping adjacent frames to view chemical events, consequently lowering the temporal resolution. This effect is even more noticeable when the contrast of the solvent or the liquid-cell TEM holder's cell window (e.g., Si_3N_4) interferes with the contrast of the observed object. Therefore, few studies have examined actual observations of atomic dynamics at millisecond frame rates, even for materials composed of heavy atoms [33].

The interaction between electron beams and molecules should also be considered from a timescale perspective. The characteristics of electrons often overlooked in TEM include

high speed (70% of light for 200 keV) and short de Broglie wavelength (2.5 picometers, $>10^{-5}$ time shorter than UV), ensuring an electron–molecule interaction to occur in <1 attosecond followed by vibrational and electronic excitations in femto- to picoseconds, and relaxation and individual reaction events of longer timescales [21]. Under SMART-EM conditions, because of a specimen's single-molecule thickness, the frequency of an electron colliding on an atom is very low [17]. The frequency of individual reaction events has been reported to occur at intervals of microseconds or longer, so each chemical event triggered by an electron is considered independent. Consequently, the dynamics of chemical reactions induced by electrons follow the first-order kinetics dependent only on the total electron dose, not the electron dose rate (EDR) per unit of time [17]. In contrast, thermal and mechanical vibrations, such as mechanical motions of molecules described in the following sections, occur independently of the electron dose irradiated.

Denoising method for high-speed single-molecule imaging

Molecular motions span a wide timescale from bond rotations in picoseconds to conformational changes of proteins in seconds. A DED camera with an in situ recording function should ideally capture sub-millisecond, high-speed, blur-free images to capture the rich dynamics of medium-sized molecules. However, increasing the imaging speed by a factor of 1000, while maintaining the same electron dose with the same sensitivity of the detector, reduces the electron dose per frame to 1/1000 and the SNR of the image. Such dim electron irradiation conditions do not provide adequate image contrast for thin organic molecules composed solely of light elements [34]. For instance, Fig. 3a presents an image of a CNT encapsulating four [60]fullerene (C_{60}) molecules, taken with a DED camera at 1600 fps [35]. The raw frame image has a low SNR of 0.05 because of

insufficient electron dose per single frame. The molecular image becomes clearer when 50 consecutive frames are overlaid via pixel averaging (Fig. 3b; SNR = 0.20), but the temporal resolution is also reduced to 31.25 msec/frame, negating the advantage of the high-speed camera.

To achieve both high temporal resolution and sufficient SNR for in situ molecular imaging, distinguishing molecular images from the background, we turned our attention to the total variation denoising method commonly used in web video compression techniques. This method compares differences between adjacent frames in a video time series and filters them to minimize the total variation of the signal. It operates on the principle that noise is in the areas of significant change, while the observed object (molecule) is in the areas of minor change. We tested several denoising methods and total variation algorithms, including various existing filtering methods, and found that the Chambolle total variation (CTV) denoising method was the most suitable for single-molecule TEM imaging applications, including SMART-EM [36].

While general denoising filters smooth the edge shapes of molecules and lose fine structural information as noise is reduced, the CTV denoising method can remove background noise while preserving edge structures, even if the SNR of the original video is low. In the CTV-denoised image (SNR = 0.15) shown in Fig. 3c, the shape of the molecule is visible even in a single frame taken at 1600 fps (= 0.625 ms/frame). When three frames are superimposed and CTV denoising is applied simultaneously (1.875 ms/frame, Fig. 4d), the spherical shape of the C_{60} molecules can be observed with an SNR = 0.30. From this image, we can obtain intermolecular distance information with an

accuracy of 0.01 nm at a speed of 1.875 sec/frame. We can then determine that the two circular images at the two ends are C_{60} molecules, while the two circular images in the center originate from a single C_{120} fullerene molecule, where two C_{60} molecules are covalently linked by electron irradiation [37].

The CTV denoising method is effective in enhancing signals that are obscured by noise in video images. It is especially effective for images obtained with scintillator-based detectors and raw video frames taken by a DED camera without an electron counting process. Fig. 4 presents an example of using CTV denoising on a SMART-EM video of a biotin molecule (vitamin B7) attached to the tip of a cone-shaped CNT via a flexible chain-like molecular entity. This example shows imaging of structural changes of a molecule. The biotin molecule (Fig. 4a) moved continuously on the CNT, providing different images in each video frame (Fig. 4b) [38]. The SNR of the image taken with a CCD camera (Gatan Ultrascan 1000) was low (0.19), and in some frames, it was even challenging to identify the molecular structure (e.g., the 31.9-sec image in Fig. 4b). However, when the CTV denoising is applied to a series of images, the molecular shapes become distinguishable from the background (SNR = 17.3), making the structural changes of the molecules visible (Fig. 4c).

Visualization of nanomechanical molecular motion

The 2016 Nobel Prize in Chemistry was awarded for the design and synthesis of molecular machines. An iconic example of these is molecular shuttles, where a shuttle (typically a ring-like structure) responds to external stimuli and moves back and forth along an axis (a guiding molecule)—a typical example of molecular machines (Fig. 5a)

[39]. This molecular shuttling motion has been traditionally observed and monitored by nuclear magnetic resonance as the average behavior of numerous molecular shuttles in a solution. However, it was not possible to witness the actual back-and-forth motion of individual molecular shuttles in response to applied stimuli such as electrons, light, and mechanical stresses.

By using a DED camera with a sub-millisecond imaging capacity and the CTV noise reduction method, we were able to visualize the motions of a molecular shuttle. We observed fullerene molecules confined in a 1.4 nm-wide single-walled carbon nanotube (CNT) moving like a shuttle. This movement in a slow-motion SMART-EM video was recorded at 1600 fps [40]. We used statistical analysis of the denoising-enhanced molecular contrast intensity using a large number of video frames as a data source. This analysis allowed us to determine the position of the molecules with exceptionally high positional and temporal precision—0.01 nm and 0.9 ms, respectively. As depicted in Fig. 5c, we observed a C_{120} molecule moving 2.79 nanometers between 3.8 and 5.6 ms after the video started. This moment was captured with millisecond temporal precision.

The driving force behind the shuttle-like motion of molecules inside carbon nanotubes (CNTs) has been speculated to be either thermal energy [28] or energy from electron beams [41]. However, these theorems lacked experimental evidence. A quantitative analysis of slow-motion videos showcasing the shuttle motion of fullerene molecules shows that the CNTs vibrate with a <1-Å amplitude, and the molecules inside react to these angstrom-level vibrations, triggering the shuttle-like motion.

As illustrated in Fig. 6a, the observed nanotube vibrations have a frequency of around 0.1 sec and an amplitude of about 1 Å. The time series plot of the molecule's position (Fig. 5b, blue) and the CNT's position (Fig. 6b, red) shown in Fig. 6c suggest that when the direction of the nanotube's vibration changes (thus maximizing the molecule's acceleration), the molecule shifts from one end to the other while rotating longitudinally because of the inertial force. This observation provides experimental evidence of the correlation between work and energy at the molecular level. The kinetic energy is transferred from the mechanically vibrating nanotubes to the molecules inside, prompting the molecules to translate and rotate. When the temperature was changed from 25 °C to 150 °C, the frequency of the shuttle motion remained largely unchanged, indicating that this motion is not induced by thermal energy.

This process is similar to the movement of pebbles inside a maraca when shaken. The pebbles move synchronously with the vibrations of the container and make a sound when they hit the container wall (Fig. 6d). The microscopic movement of molecules, as observed by SMART-EM, mirrors this macroscopic phenomenon, demonstrating that the mechanical behaviors we commonly see in our macroscopic world also exist in the nanoscopic realm.

The millisecond-scale TEM imaging aids in understanding the dynamic behavior of molecules at the nanoscale and in interpreting TEM images of individual molecules and molecular assemblies. Often, atomic-resolution images of single molecules taken with second-long exposures do not match predicted TEM simulations and appear more blurred. This discrepancy is more evident when molecules are loosely attached to the CNT surface

via covalent or non-covalent interactions.

To understand the cause of this discrepancy, a SMART-EM video of cyclodextrin (CD, a cyclic oligomer of D-glucose) bound to the tip of a conical CNT through host–guest interactions was recorded at a frame rate of 400 fps (Fig. 7a and b) [42]. The results demonstrated that cyclodextrin molecules undergo rotational and conformational changes on a millisecond scale (Fig. 7c). Interestingly, the TEM experimental image obtained from a single 0.625 ms frame closely resembled the simulated TEM image shown in Fig. 7b, whereas the image obtained by second-long exposure (Fig. 7d) does not match the TEM simulations. This result suggests that for flexible and mobile molecules, the single-molecule image in sub-second-scale SMART-EM imaging is essentially a composite of information from multiple conformations. A similar conclusion was also drawn from SMART-EM images of the cyclic peptide daptomycin covalently bonded to a conical CNT [43].

Short exposure time SMART-EM imaging is a crucial technology for the precise 3D structure determination of complex organic molecules and molecular assemblies that may have multiple conformational configurations. To enhance its utility, it is essential to further improve the SNR by employing high-sensitivity sensors and refined image processing techniques.

Monitoring multistep chemical reaction at sub-millisecond resolution

SMART-EM technologies allow for the observation of molecular motions and the study of chemical reactions. The dimerization of van der Waals (vdW) dimers of C_{60} molecules

to form short CNTs is a frequently studied reaction in the field of carbon chemistry. This dimerization reaction has been observed under a variety of conditions: high pressure [44], high temperature [45,46], metal reduction [47], photo and electron irradiation [48,49], and catalytic mechanochemical conditions [37]. The reaction is useful in the precise synthesis of double-walled CNTs from fullerene peapods [50].

During this reaction, adjacent C_{60} molecules initially form a dumbbell-shaped dimer (C_{120}) and subsequently transform into a larger spherical molecule. This transformation is driven by the release of the distortion in the π-conjugation of the C_{60} molecule. In reactions triggered by electron beams or light, this transformation involves an electronically excited state. Although the conversion from C_{60} to a spherical molecule involves multiple steps of carbon–carbon bond cleavage and reforming, conventional TEM techniques, which have second-scale time resolution, have found it challenging to identify each step of the reaction and to experimentally investigate the reaction mechanism [17,51].

To address this, we performed 1600 fps SMART-EM imaging to continuously monitor the cascade dimerization of a single vdW dimer of C_{60} [52]. Along with the CTV denoising algorithm, we also used an automatic XC image-matching analysis of density functional theory (DFT)-based TEM simulations. This combination of techniques allowed us to identify the shape and size of intermediates and to determine the lifetime of each intermediate.

The shortest pathway for the transformation from van der Waals (vdW) dimer to D_{5d}

symmetric (5,5) CNT (OT-24) has been proposed to be a series of Stone–Wales rearrangements by Osawa and Tomanek based on theoretical calculations [53]. This process begins with the vdW dimer (named OT-0 in the original paper) and ends in OT-24 (Fig. 8a). The initial step is a retro [2 + 2] cycloaddition of OT-1, resulting in a distorted 12-membered ring in OT-2. This is the highest energy and longest C_{60}–C_{60} distance stage at 0.94 ± 0.02 nm. Following this, the C_{60}–C_{60} distance decreases and the system stabilizes energetically after OT-6. However, OT-2, with its high energy requirement (282 kJ/mol) for conversion from OT-1, is expected to be barely detectable in the cascade reaction. High energy reactive species are often important in chemical reactions, but verifying these intermediates is difficult in bulk experiments because of their short lifetimes and complex structures.

In Fig. 8b, four images are shown from a 62.5 ms/frame SMART-EM video of the electron-beam-induced transformation of C_{60} molecules. The distances of C_{60} molecule pairs 1–2, 3–4, 4–5, and 5–6 range from 0.97 to 1.08 nm, implying that the molecules are either in vdW contact or slightly apart. However, the distance of the pair 2–3 is 0.80 nm, indicating that these two molecules have reacted prior to the TEM video recording starting, forming a “peanut-shaped” dimer. Notably, the distance between pair 4–5 decreased from 1.01 nm to 0.91 nm between the 62.5 and 125.0 ms frames, suggesting that the [2 + 2] cycloaddition reaction occurred during this period.

To pinpoint when the cycloaddition occurred, CTV denoising was applied to the faster video frames from 125.5 to 187.5 ms. From Fig. 8c, a reduction in the 4–5 distance can be observed between the 122.5–135.0 ms frames. Further temporal resolution obtained

from the 1.25 ms/frame video frames shown in Fig. 8d revealed that the [2 + 2] cycloaddition reaction occurred between the 127.5–128.8 ms and 128.8–130.0 ms frames. This means that the reaction event can be reliably determined with a time precision of up to 1.25 ms. The average distance *d* of the [2 + 2] cycloadduct was found to be 0.91 ± 0.02 nm, which aligns well with that obtained from X-ray structure analysis. This suggests that the distance measurement from the 1.25 ms/frame video data is highly accurate [37].

The next step to derive meaningful chemical insights from high-speed SMART-EM videos is to determine the molecular structure in each video frame. To accomplish this, we compared the distances and geometries from experimental data to those of molecular models from DFT calculations and TEM image simulations, thereby assigning intermediate structures (Fig. 9). A library of 864 simulated TEM images was created by rotating 24 potential structural candidates of the C_{120} molecules along the long axis and capturing the projections from various angles (Fig. 9a). Using XC analysis, we quantified the similarity between each simulated and experimental TEM image to estimate the structure of the C_{120} molecule at different time points. This technique enabled the identification of short-lived chemical intermediates with lifetimes in the millisecond range.

The aforementioned structure determination technique, combined with the estimation of structures based on intermolecular distance information, allowed us to quantify when each intermediate appeared and disappeared during the conversion of C_{60} to the fused dimer. Fig. 9b illustrates the time-dependent conversion from OT-0 to OT-14 at 423 K, with the distance *d* measured every 3.125 ms. The first intermediate to appear was

identified as OT-1 because of its measured distance (0.90 nm), consistent with the known distance from crystal structure data of OT-1, a [2 + 2] cycloadduct. Following the formation of OT-1, the distance initially increased to 0.95 nm and subsequently decreased in roughly three steps to 0.90 nm, 0.84 nm, and 0.80 nm. The OT-2 intermediate, with a unique length and extremely short lifetime of <3 ms, was observed at d = 0.95 nm. This intermediate was detected in only three out of dozens of molecules examined via video imaging.

The OT-4 intermediate, being at a local energy minimum, is expected to have a longer lifetime and was found experimentally to appear between 20 ms and 45 ms at d = 0.90 nm. The intermediate observed at d = 0.84 nm aligned well with OT-11 (Fig. 9c), although there may be an overlap with intermediates from OT-8 to OT-11, which are difficult to distinguish in the TEM simulation image. The species appearing at 78 ms, an intermediate with the longest lifetime of 40 ms, was assigned as OT-14. This long-lived d = 0.80 nm intermediate, along with the vdW dimer OT-0 and the [2 + 2] cycloadduct OT-1, has been often reported in the literature as a "peanut-shaped" dimer [54,55,56]. However, its precise structural identification was achieved for the first time by comparison with simulated images using millisecond SMART-EM analysis (Fig. 9c).

Statistical in situ TEM observations of the C_{60} fusion reaction were conducted on video datasets obtained for dozens of molecules, yielding three significant conclusions. First, multiple independent experiments identified the OT-2 intermediate. This verification confirmed that OT-2 was not a misidentified artifact, but a kinetically trapped

intermediate with a relatively high energy barrier between OT-2 and OT-3. Second, the reaction events were found to be purely stochastic and influenced by the variable lifetime of each metastable intermediate. After organizing almost a million 0.625-ms frames, the timing of a single reaction event could be pinpointed with a minimum precision of 1.25 ms. Third, the same sequence of intermediates was detected at both 298 K and 423 K, indicating that the pathway proposed by Osawa and Tomanek is valid in both temperature regimes [53].

These results provide experimental support for the theoretically proposed reaction mechanisms of nanocarbons and highlight the capabilities of SMART-EM to study molecular events with sub-millisecond and sub-angstrom precision. For instance, the chemical transformation of nanocarbons inside CNTs models the formation of amorphous regions in the gaps between crystalline graphite regions of carbon fibers (CF). Recently, we reported in situ and ex situ visualization of carbon fiber formation reaction in CNTs by pyrolysis of polyacrylonitrile (PAN) [57]. The studies suggested that the formation of high-entropy structures comprising curved graphene-like structures containing five- and seven-membered carbon rings underlies the unique material properties, such as the high tensile strength of PAN-derived CF. Therefore, high-speed atomic-resolution imaging can also contribute to understanding the structure-property relationship of bulk materials at the atomic level.

Nucleation and epitaxial growth processes of sodium chloride

SMART-EM is not limited to studying organic and carbon materials; it also provides unprecedented insights into the dynamics of inorganic nanomaterials, such as

crystallization. The crystallization of rock salt, or sodium chloride (NaCl), is a method of refining materials that humans have likely used since prehistoric times. It is also the most well-known crystallization phenomenon widely used as experimental material in primary education worldwide. Using the SMART-EM method, the emergence of NaCl crystal nuclei in a vacuum of conical CNTs and their stepwise epitaxial growth into rectangular nano-sized crystals were captured as a video [58]. In a series of 150-sec TEM videos taken with a CMOS camera at a frame rate of 25 fps (Fig. 10), the precise moment of NaCl nucleation and the subsequent crystal growth process were observed nine times. Each event lasted from a few seconds to 20 seconds.

Much like the tubular CNTs described, the conical CNTs also demonstrated repeated oscillations with an amplitude of about 1 Å under SMART-EM observation. This mechanical stimulation caused the molecular aggregates to grow and move to the base of the CNTs. During each nucleation event, the nucleus appeared in an orderly fashion composed of 48 sodium and 48 chlorine atoms. However, the timing of the appearance of the crystal nuclei followed a normal distribution, meaning that nucleation events are probabilistic in nature and occur at random intervals around an average time.

With a temporal resolution of 25 fps, it was challenging to obtain sufficient experimental data on the individual atomic-level dynamics of NaCl growth on the surface of the nanocrystal. Thus, in situ imaging with a DED camera allows for the observation of NaCl crystal growth dynamics at a temporal resolution of 3.38 ms/frame [59]: a tenfold increase in imaging speed compared to previous conditions. The resulting TEM video data of two-dimensional nucleation on defect-free NaCl nanocrystals within CNTs captures the

formation of a metastable floating island (FI) that thermally moves onto the (100) plane of NaCl, representing the first step of epitaxial growth.

Fig. 11a illustrates how, in two consecutive frames of 64.19 ms, a new layer (#9) is formed on the (100) plane of the 8 × 9 nano-NaCl crystal, resulting in a 9 × 9 nanocrystal tightly anchored inside the CNT. As seen in the atomic-resolution image, layer #8 is flat and free of defects. Fig. 11b displays eight frames from the video captured at a frame rate of 3.38 ms/frame over a total of 2 sec, demonstrating the formation and thermal transfer of FI and the time evolution of the epitaxy of layer #9 on #8 for approximately 1.7 sec (–1542.45 to 114.92 ms). Events of FI formation, and hence crystal growth events, on defect-free (100) planes were analyzed for several nanocrystals and found to be completely stochastic and rare, occurring only once every 2 to 10 sec or longer. This observation offers experimental support at the atomic level for the idea that nucleation on defect-free crystal faces is an unfavorable process, a fact often suggested in the literature [60,61].

Distance measurements based on video data with millisecond-scale time resolution provide temporal and spatial statistical information about the dynamics of the FI, data not attainable via conventional experimental methods: At 3.38 ms, the first FI formed has a length (l) of 0.5 nm, equivalent to one unit of NaCl (Fig. 11c). Mapping the migration over time reveals that the minimum rates of migration at 298 K are estimated to be about 0.3 nm ms^{-1}. The most characteristic parameter is the large interlayer distance d, averaging 0.34 nm (Fig. 10d). This value of d is 23% longer than the bulk crystal value (0.282 nm), indicating that the FI floats on atomically flat (100) facets. At 81.12 ms, the FI contacts the left wall of the CNT, loses kinetic energy, and lands on layer #8. As this,

FI forms as the last metastable species before irreversible crystal growth starts, and it can be regarded as a critical crystal nucleus for two-dimensional epitaxy. Because this FI is no longer floating, it must be considered a terrace. This terrace began to grow rapidly into a new layer #9 at 94.92 ms and was completed in about 30 ms (Fig. 11c).

The floating FI on the (100) facet with d = 0.341 nm results from the large lattice size discrepancy between a single-layer NaCl and NaCl crystals. A single-layer NaCl ion pair with an interatomic distance of 0.234 nm is 17% shorter than the 0.282 nm distance found in the crystal (Fig. 11e). As the cluster size increases, the inter-ion interaction weakens, and the distance expands to 0.272 nm (4% shorter) for $(NaCl)_8$ and 0.277 nm (2%) for $(NaCl)_{18}$ (i.e., 6 × 6 cluster). Because a lattice mismatch of 5% or less favors epitaxy [62,63,64,65,66], the $(NaCl)_8$ cluster could only have landed when it lost kinetic energy upon contacting the left CNT wall at 81.12 ms.

Millisecond SMART-EM imaging has also successfully captured examples of mobile epitaxy via a FI confined in the space between the nanocrystal and the CNT wall. This space acts as a capillary, housing ion pairs because of the reduced effective surface energy [67]. In the left frame of Fig. 11a, taken over 3.38 ms, we observe a (6,8) crystal with a 5-ion long shoulder as layer #7. In the next frame, this layer has disappeared, and the nanocrystal has grown only one layer in the y direction. As depicted in Fig. 11b, this migration happened swiftly during the 3.38 ms interval. Moreover, by quantitatively measuring the time variation of CNT vibration and crystal growth, the low-frequency mechanical vibration of the CNT container drives the mobile two-dimensional epitaxy (Fig. 11c). A curve-fitting simulation of the CNT vibration (Fig. 11d) revealed that the

acceleration of CNT motion is extremely small (4.4 femtometers ms^{-1}); thus, the force exerted on the FI should also be extremely small.

When crystals tumble in a container, a space is repeatedly formed between the crystals and the container wall that hosts the FI. The repeated tumbling alters the surface energy and promotes the transformation of the FI into new epitaxial layers (Fig. 11e right). This is a completely different surface crystal growth mechanism from conventional on-site epitaxy (Fig. 11e left), and this surface catalytic mechanism, discovered at the nanoscale, is expected to operate in bulk heterogeneous nucleation, where crystallization is enhanced by stirring.

Conclusion

The 20th century was the era of cinema, but the potential of high-resolution molecular imaging in chemistry was largely overlooked. Now, the SMART-EM method heralds a breakthrough, allowing us to observe the dynamic motions and reactions of individual molecules with atomic-level detail. This technology enhances the image quality of high-speed video frames and enables precise measurement of distances between individual molecules and ions during the epitaxial growth of crystals.

Despite these advancements, SMART-EM's current sub-millisecond imaging speed is insufficient for capturing wider-scale molecular dynamics [68,69]. However, the advent of high-speed electrostatic beam blanking and deflection technology promises to extend observations to nanosecond and microsecond timescales, expanding SMART-EM's applications in the near future.

The inherently chaotic nature of molecular motion and chemical reactions has always posed a challenge for the experimental tracking of individual molecules. However, the SMART-EM technique, by providing a 'cinematic' view of chemistry, can reveal chemical phenomena that deviate significantly from the average. This represents a significant stride in bridging the gap between thermodynamics and statistical mechanics and between chemical research and education.

Acknowledgements

The authors appreciate the experimental and intellectual contributions of the coworkers, whose names are found in the references.

Funding

This work was supported by Japan Society for the Promotion of Science JSPS KAKENHI [grant numbers JP19H05459, JP21H01758, JP22K14704, and JP23H04874]; Japan Science and Technology Agency (JST) SENTAN [grant number JPMJSN16B1]; and JST CREST [grant number JPMJCR20B2].

References

1 https://archive.org/details/muybridgescomple03muyb/page/1268/mode/2up

2 Uyeda N, Kobayashi T, Ishizuka K, Fujiyoshi Y (1978/79) High voltage electron microscopy for image discrimination of constituent atoms in crystals and molecules. *Chemica Scripta.* **50:** 47–61.

3 Uyeda N, Kobayashi T, Ishizuka K, Fujiyoshi Y (1980) Crystal structure of Ag·TCNQ. *Nature* **285**: 95.

4 Shen B, Wang H, Xiong H, Chen X, Bosch E G T, Lazić I, Qian W, Wei F (2022) Atomic imaging of zeolite-confined single molecules by electron microscopy. *Nature* **607:** 703–707.

5 Xing J, Takeuchi K, Kamei K, Nakamuro T, Harano K, Nakamura E (2022) Atomic-number (Z)-correlated atomic sizes for deciphering electron microscopic molecular images. *Proc. Natl. Acad. Sci*. **119:** e2114432119.

6 Ando T (2018) High-speed atomic force microscopy and its future prospects. *Biophys Rev.* **10**: 285–292.

7 Uchihashi T, Iino R, Ando T, Noji H (2011) High-Speed Atomic Force Microscopy Reveals Rotary Catalysis of Rotorless F1-ATPase. *Science* **333:** 755–758.

8 Nakamura E, Sommerdijk N A J M, Zheng H (2017) Transmission electron microscopy for chemists. *Acc. Chem. Res.* **50:** 1795–1796.

9 Koshino M, Tanaka T, Solin N, Suenaga K, Isobe H, Nakamura E (2007) Imaging of single organic molecules in motion. *Science* **316:** 853.

10 Liu Z, Yanagi K, Suenaga K, Kataura H, Iijima S (2007). Imaging the dynamic behaviour of individual retinal chromophores confined inside carbon nanotubes. *Nat. Nanotechnol.* **2**: 422–425.

11 Lungerich D, Hoelzel H, Harano K, Jux N, Amsharov K Yu, Nakamura E (2021) A singular molecule-to-molecule transformation on video: The bottom-up synthesis of fullerene C_{60} from truxene derivative $C_{60}H_{30}$. *ACS Nano* **15:** 12804–12814.

12 Hoelzel H, Lee S, Amsharov K Yu, Jux N, Harano K, Nakamura E, Lungerich D

(2023) Time-resolved imaging and analysis of the electron beam-induced formation of an open-cage metallo-azafullerene. *Nat. Chem.* DOI: 10.1038/s41557-023-01261-7.

13 Cao K, Skowron S T, Biskupek J, Stoppiello C T, Leist C, Besley E, Khlobystov A N, Kaiser U (2020) Imaging an unsupported metal–metal bond in dirhenium molecules at the atomic scale. *Sci. Adv.* **6**: eaay5849.

14 Chuvilin A, Bichoutskaia E, Gimenez-Lopez M C, Chamberlain T W, Rance G A, Kuganathan N, Biskupek J, Kaiser U, Khlobystov A N (2011) Self-assembly of a sulphur-terminated graphene nanoribbon within a single-walled carbon nanotube. *Nat. Mater.* **10**: 687–692.

15 Cao K, Biskupek J, Stoppiello C T, McSweeney R L, Chamberlain T W, Liu Z, Suenaga K, Skowron S T, Besley E, Khlobystov A N, Kaiser U (2020). Atomic mechanism of metal crystal nucleus formation in a single-walled carbon nanotube. *Nat. Chem.* **341**: 855.

16 Skowron S T, Chamberlain T W, Biskupek J, Kaiser U, Besley E, Khlobystov A N (2017) Chemical reactions of molecules promoted and simultaneously imaged by the electron beam in transmission electron microscopy. *Acc. Chem. Res.* **50:** 1797–1807.

17 Okada S, Kowashi S, Schweighauser L, Yamanouchi K, Harano K, Nakamura E (2017) Direct microscopic analysis of individual C_{60} dimerization events: Kinetics and mechanisms. *J. Am. Chem. Soc.* **139:** 18281–18287.

18 Nakamura E, Harano K (2018) Chemical kinetics study through observation of individual reaction events with atomic-resolution electron microscopy. *Proc. Jpn. Acad. Ser. B* **94:** 428–440.

19 Liu D, Kowashi S, Nakamuro T, Lungerich D, Yamanouchi K, Harano K, Nakamura

E (2022) Ionization and electron excitation of C_{60} in a carbon nanotube: A variable temperature/voltage transmission electron microscopic study. *Proc. Natl. Acad. Sci*. **119:** e2200290119.

20 Egerton R F (2019) Radiation damage to organic and inorganic specimens in the TEM. *Micron* **119:** 72–87.

21 Turro N J, Ramamurthy V, Scaino J C (2009) "Molecular Photochemistry of Organic Compounds: An Overview" in *Principles of Molecular Photochemistry: An Introduction*, N. J. Turro, V. Ramamurthy, J. C. Scaino, Eds. (University Science Books, Melville, NY), pp. 1–38.

22 Harano K, Takenaga S, Okada S, Niimi Y, Yoshikai N, Isobe H, Suenaga K, Kataura H, Koshino M, Nakamura E (2014) Conformational analysis of single perfluoroalkyl chains by single-molecule real-time transmission electron microscopic imaging. *J. Am. Chem. Soc.* **136**: 466–473.

23 https://microscopy.or.jp/jsm/wp-content/uploads/EM5_project.pdf

24 Zewail A H (2010) Four-dimensional electron microscopy. *Science* **328:** 187–193.

25 Zewail A H, Thomas J M (2010) *4D Electron Microscopy: Imaging in Space and Time.* (Imperial College Press).

26 Ischenko A A, Weber P M, Miller R J D (2017) Capturing chemistry in action with electrons: Realization of atomically resolved reaction dynamics. *Chem. Rev.* **117**: 11066–11124.

27 Li X, Zheng S Q, Egami K, Agard D A, Cheng Y (2013) Influence of electron dose rate on electron counting images recorded with the K2 camera. *J. Struct. Biol.* **184:** 251–260.

28 Warner J H, Ito Y, Ruemmeli M H, Buechner B, Shinohara H, Briggs G A D (2009) Capturing the motion of molecular nanomaterials encapsulated within carbon nanotubes with ultrahigh temporal resolution. *ACS Nano* **3**: 3037–3044.

29 Liao H G, Zherebetskyy D, Xin H, Czarnik C, Ercius P, Elmlund H, Pan M, Wang L W, Zheng H (2014) Facet development during platinum nanocube growth. *Science* **345:** 916–919.

30 Alcorn F M, Jain P K, van der Veen R M (2023) Time-resolved transmission electron microscopy for nanoscale chemical dynamics. *Nat. Rev. Chem.* **7:** 256–272.

31 Poerwoprajitno A R, Gloag L, Watt J, Cheong S, Tan X, Lei H, Tahini H A, Henson A, Subhash B, Bedford N M, Miller B K, O'Mara P B, Benedetti T M, Huber D L, Zhang W, Smith S C, Gooding J J, Schuhmann W, Tilley R D (2022) A single-Pt-atom-on-Ru-nanoparticle electrocatalyst for CO-resilient methanol oxidation. *Nat. Catal.* **5:** 231–237.

32 Zakharov D N, Bedewy M, Balakrishnan V, Pattinson S W, Meshot E R, Hart A J, Stach E A (2015) Fast imaging of carbon nanotube carpet growth by environmental TEM. *Microsc. Microanal*. **21:** 2327–2328.

33 Radetic T, Gautam A, Ophus C, Czarnik C, Dahmen U (2014) High resolution observations of interface dynamics using a direct electron detection camera. *Microsc. Microanal.* **20:** 1594–1595.

34 Xing J, Takeuchi K, Kamei K, Nakamuro T, Harano K, Nakamura E (2022) Atomic-number (*Z*)-correlated atomic sizes for deciphering electron microscopic molecular images. *Proc. Natl. Acad. Sci. USA*. **119:** e2114432119.

35 Stuckner J, Shimizu T, Harano K, Nakamura E, Murayama M (2020) Ultra-fast

electron microscopic imaging of single molecules with a direct electron detection camera and noise reduction. *Microsc. Microanal.* **26:** 667–675.

36 Chambolle A (2004) An algorithm for total variation minimization and applications. *J. Math. Imaging Vis.* **20:** 89–97.

37 Wang G W, Komatsu K, Murata Y, Shiro M (1997) Synthesis and X-ray structure of dumb-bell-shaped C_{120}. *Nature* **387:** 583–586.

38 Gorgoll R M, Yücelen E, Kumamoto A, Shibata N, Harano K, Nakamura E (2015) Electron microscopic observation of selective excitation of conformational change of a single organic molecule. *J. Am. Chem. Soc.* **137:** 3474–3477.

39 Silvi S, Venturi M, Credi A (2009) Artificial molecular shuttles: from concepts to devices. *J. Mater. Chem.* **19:** 2279–2294.

40 Shimizu T, Lungerich D, Stuckner J, Murayama M, Harano K, Nakamura E (2020) Real-time video imaging of mechanical motions of a single molecular shuttle with sub-millisecond sub-angstrom precision. *Bull. Chem. Soc. Jpn.* **93:** 1079–1085.

41 Smith B W, Monthioux M. Luzzi D. E. (1999) Carbon nanotube encapsulated fullerenes: a unique class of hybrid materials. *Chem. Phys. Lett.* **315:** 31–36.

42 Hanayama H, Yamada J, Tomotsuka I, Harano K, Nakamura E (2021) Rim binding of cyclodextrins in size-sensitive guest recognition. *J. Am. Chem. Soc.* **143:** 5786–5792.

43 Nakamuro T, Kamei K, Sun K, Bode J W, Harano K, Nakamura E (2022) Time-resolved atomistic imaging and statistical analysis of daptomycin oligomers with and without calcium ions. *J. Am. Chem. Soc*. **144:** 13612–13622.

44 Núñez-Regueiro M, Marques L, Hodeau J L, Béthoux O, Perroux M (1995) Polymerized fullerite structures. *Phys. Rev. Lett.* **74:** 278–281.

45 Bandow S, Takizawa M, Hirahara K, Yudasaka M, Iijima S (2001) Raman scattering study of double-wall carbon nanotubes derived from the chains of fullerenes in single-wall carbon nanotubes. *Chem. Phys. Lett.* **337:** 48–54.

46 Yeretzian C, Hansen K, Diederichi F, Whetten R L (1992) Coalescence reactions of fullerenes. *Nature* **359:** 44–47.

47 Komatsu K, Wang G W, Murata Y, Tanaka T, Fujiwara K, Yamamoto K, Saunders M (1998) Mechanochemical synthesis and characterization of the fullerene dimer C_{120}, *J. Org. Chem*. **63:** 9358–9366.

48 Rao A M, Zhou P, Wang K A, Hager G T, Holden J M, Wang Y, Lee W T, Bi X X, Eklund P C, Cornett D S (1993) Photoinduced polymerization of solid C_{60} films. *Science* **259:** 955–957.

49 Hernández E, Meunier V, Smith B W, Rurali R, Terrones H, Nardelli M B, Terrones M, Luzzi D E, Charlier J C (2003) Fullerene coalescence in Nnnopeapods: A path to novel tubular carbon, *Nano Lett*. **3:** 1037–1042.

50 Kalbáč M, Kavan L, Juha L, Civiš S, Zukalová M, Bittner M, Kubát P, Vorlíček V, Dunsch L (2005) Transformation of fullerene peapods to double-walled carbon nanotubes induced by UV radiation. *Carbon* **43:** 1610–1616.

51 Koshino M, Niimi Y, Nakamura E, Kataura H, Okazaki T, Suenaga K, Iijima S, (2010) Analysis of the reactivity and selectivity of fullerene dimerization reactions at the atomic level. *Nat. Chem*. **2:** 117–124.

52 Shimizu T, Lungerich D, Harano K, Nakamura E (2022) Time-resolved imaging of stochastic cascade reactions over a submillisecond to second time range at the angstrom level. *J. Am. Chem. Soc.* **144:** 9797–9805.

53 Han S, Yoon M, Berber S, Park N, Ōsawa E, Ihm J, Tománek D (2004) Microscopic mechanism of fullerene fusion. *Phys. Rev. B*. **70:** 113402.

54 Smith B W, Luzzi D E (2000) Formation mechanism of fullerene peapods and coaxial tubes: a path to large scale synthesis. *Chem. Phys. Lett*. **321**: 169–174.

55 Bandow S, Takizawa M, Hirahara L, Yudasaka M, Iijima S (2001) Raman scattering study of double-wall carbon nanotubes derived from the chains of fullerenes in single-wall carbon nanotubes. *Chem. Phys. Lett*. **337:** 48–54.

56 Mirzayev R, Mustonen K, Monazam M R A, Mittelberger A, Pennycook T J, Mangler C, Susi T, Kotakoski J, Meyer J C (2017) Buckyball sandwiches. *Sci. Adv.* **3:** e1700176.

57 Ishikawa T, Tanaka F, Kurushima K, Yasuhara A, Sagawa R, Fujita T, Yonesaki R, Iseki K, Nakamuro T, Harano K, Nakamura E (2023) Wavy graphene-like network forming during pyrolysis of polyacrylonitrile into carbon fiber. *J. Am. Chem. Soc.* **145:** 12244–12254.

58 Nakamuro T, Sakakibara M, Nada H, Harano K, Nakamura E (2021) Capturing the moment of emergence of crystal nucleus from disorder. *J. Am. Chem. Soc.* **143**: 1763–1767.

59 Sakakibara M, Nada H, Nakamuro T, Nakamura E (2022) Cinematographic recording of a metastable floating island in two- and three-dimensional crystal growth. *ACS Cent. Sci.* **8:** 1704–1710.

60 Vekilov P G (2007) What determines the rate of growth of crystals from solution? *Cryst. Growth Des.* **7:** 2796–2810.

61 Pusey M L, Snyder R S, Naumann R (1986) Protein crystal growth. Growth kinetics

for tetragonal lysozyme crystals. *J. Biol. Chem.* **261:** 6524–6529.

62 Tóth G I, Tegze G, Pusztai T, Gránásy L (2012) Heterogeneous crystal nucleation: The effect of lattice mismatch. *Phys. Rev. Lett.* **108:** 025502.

63 Kawai S, Benassi A, Gnecco E, Söde H, Pawlak R, Feng X, Müllen K, Passerone D, Pignedoli C A, Ruffieux P, Fasel R, Meyer E (2016) Superlubricity of graphene nanoribbons on gold surfaces. *Science* **351:** 957–961.

64 Gabrys P A, Seo S E, Wang M X, Oh E, Macfarlane R J, Mirkin C A (2018) Lattice mismatch in crystalline nanoparticle thin films. *Nano Lett.* **18:** 579–585.

65 Oh M H, Cho M G, Chung D Y, Park I, Kwon Y P, Ophus C, Kim D, Kim M G, Jeong B, Gu X W, Jo J, Yoo J M, Hong J, McMains S, Kang K, Sung Y E, Alivisatos A P, Hyeon T (2020) Design and synthesis of multigrain nanocrystals via geometric misfit strain. *Nature* **577:** 359–363.

66 Barrett W T, Wallace W E (1954) Studies of NaCl-KCl solid solutions. I. Heats of formation, lattice spacings, densities, schottky defects and mutual solubilities. *J. Am. Chem. Soc.* **76:** 366–369.

67 Auyeung E, Li T I N G, Senesi A J, Schmucker A L, Pals B C, de la Cruz M O, Mirkin C A (2014) DNA-mediated nanoparticle crystallization into Wulff polyhedra. *Nature* **505:** 73–77.

68 Xing J, Schweighauser L, Okada S, Harano K, Nakamura E (2019) Atomistic structures and dynamics of prenucleation clusters in MOF-2 and MOF-5 syntheses. *Nat. Commun.* **10:** 3608.

69 Nakamura E, Harano K (2018) Chemical kinetics study through observation of individual reaction events with atomic-resolution electron microscopy. *Proc. Jpn. Acad., Ser. B*, **94:** 428–440.

Figures and Legends

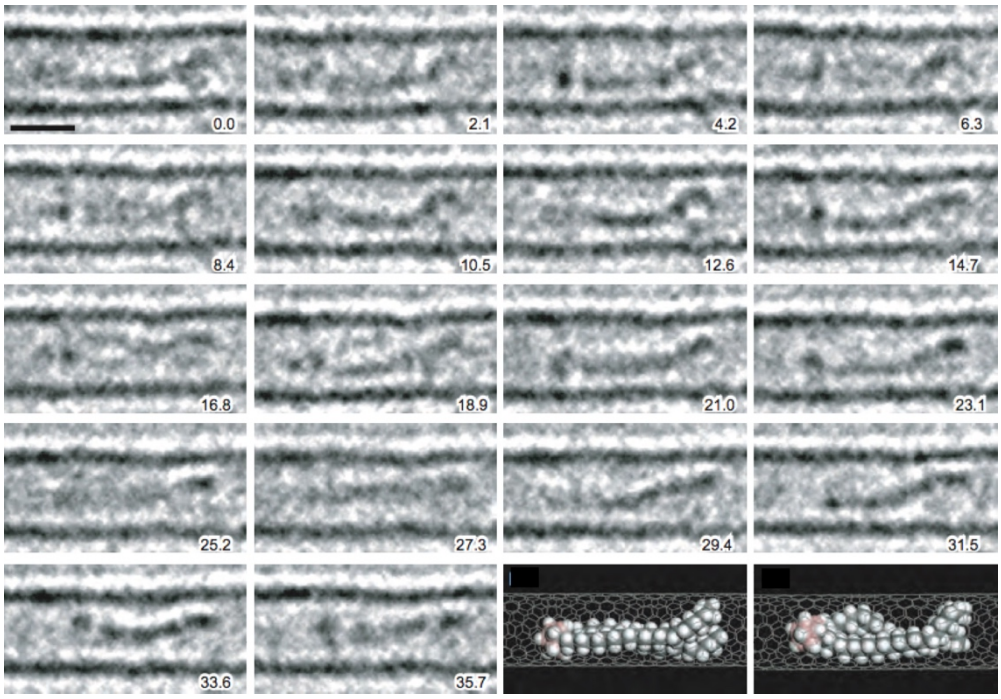

Fig. 1. A series of electron microscopic images of a dialkylated carborane molecule changing their structures in a single-walled CNT. Numbers denote the time in seconds from the start of the observation. Adapted with permission from Ref. 9.

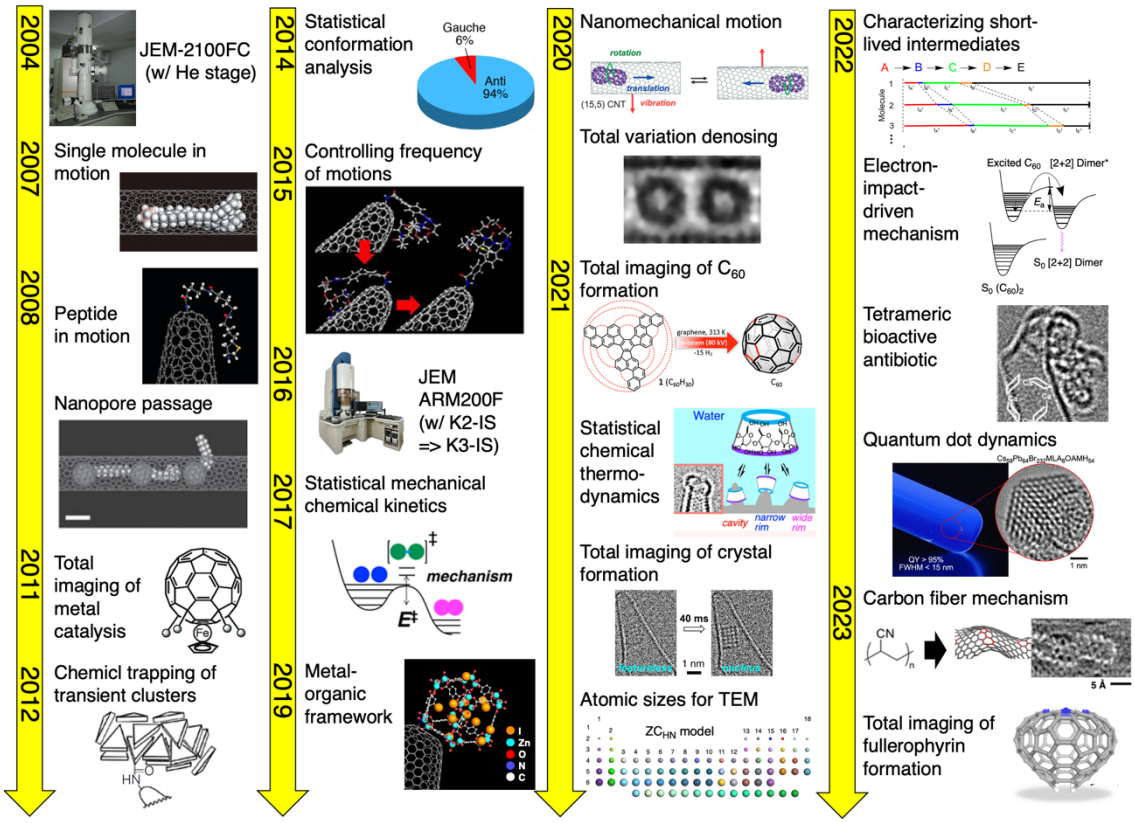

Fig. 2. History of SMART-EM studies, beginning with cinematographic studies of chemical events at atomic resolution and plunging into statistical studies on the kinetics and thermodynamics of atoms and molecules

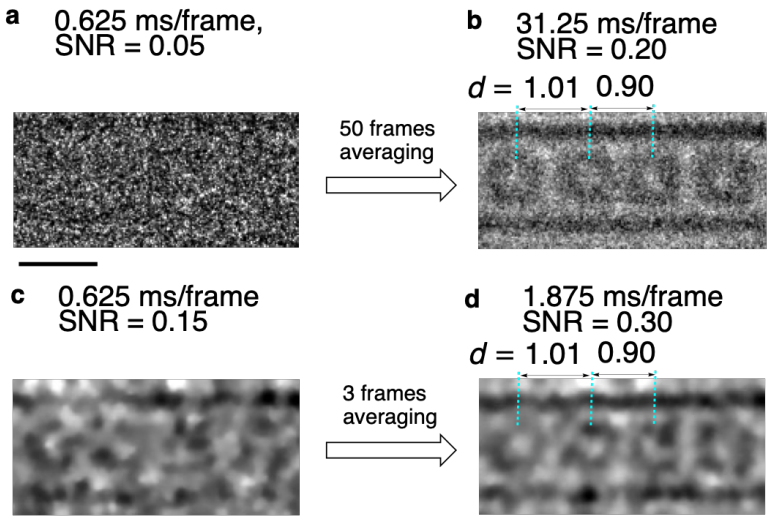

Fig. 3. Sub-millisecond-scale SMART-EM imaging and the effect of CTV noise reduction. (a) Raw image of C_{60} molecules in CNT taken with a DED camera at 0.625 ms/ frame (EDR = 2.1×10^7 e^- nm^{-2} s^{-1}). (b) Superimposed image of 50 frames, where the distance (*d*) between C_{60} molecules is shown in nm. (c) Single-frame image of (a) with CTV denoising. (d) Superimposed 3-frame image with CTV denoising. The scale bar is 1 nm. Adopted with permission from Ref. 35.

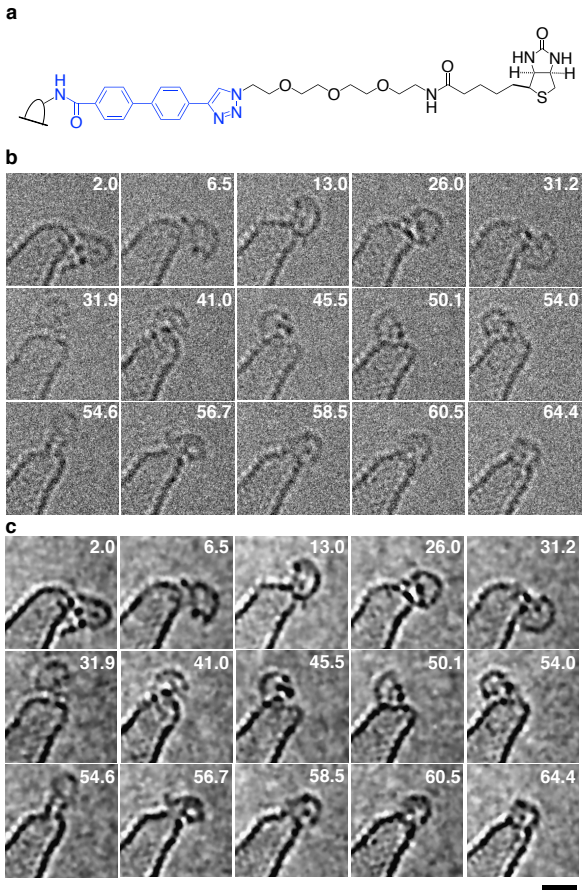

Fig. 4. Video noise removal of biotin molecules bound to a conical CNT. (a) Structure of the biotin molecule observed. (b) Raw images of video frames of a biotin molecule (acceleration voltage 80 kV, exposure time 0.4 s per frame, EDR = 2.5×10^6 e^- nm^{-2} s^{-1}). The numbers represent the time (in seconds) after the start of the movie capture. (c) Image

b with CTV denoising. The scale bar is 1 nm. Adapted with permission from Ref. 35.

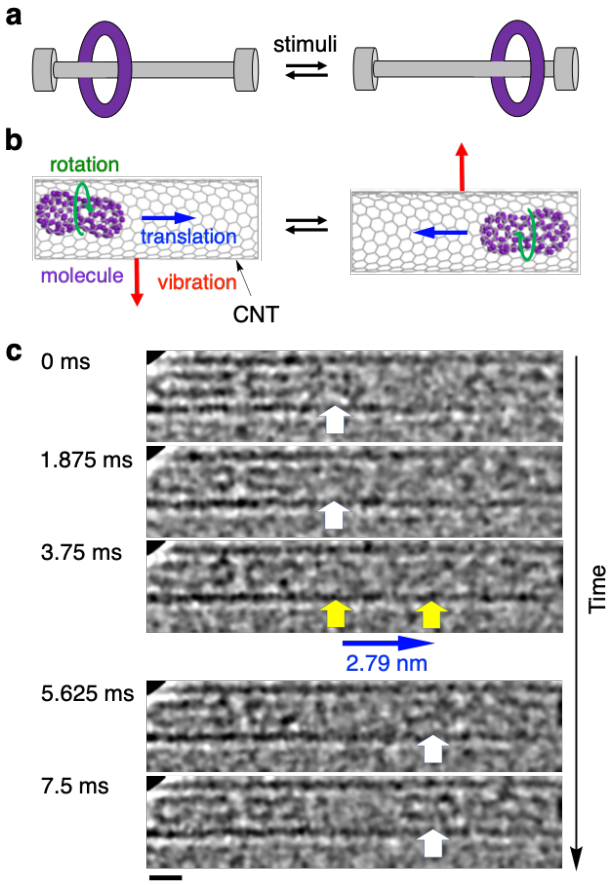

Fig. 5. High-speed SMART-EM imaging of a molecular shuttle composed of fullerene molecules and CNT. (a) Conceptual diagram of the molecular shuttle. (b) Schematic diagram of molecular shuttle motion of a fullerene molecule in a vibrating CNT. (c) Frames of SMART-EM video showing the moment of translational (shuttling) motion of a C_{120} molecule in CNT (EDR = 1.4×10^7 e^- nm^{-2} s^{-1}). The position of the C_{120} molecule is indicated by an arrow; the molecule moved translationally during the exposure of the frame after 3.8 ms (yellow arrows indicate the position before and after the movement). The scale bar is 1 nm. Adopted with permission from Ref. 40.

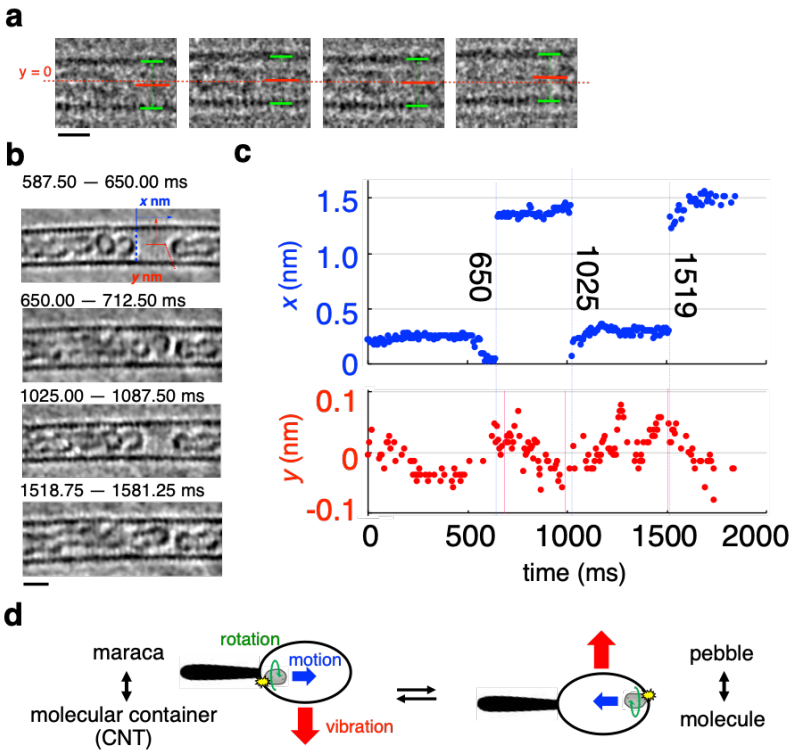

Fig. 6. Shuttling motion of fullerene molecules in conjunction with nanoscale vibration of CNT. (a) Sequential electron microscope image of a vibrating CNT. (b) SMART-EM video frames of a shuttling fullerene oligomer in response to the lateral vibration of CNT. (c) Oligomer translation (blue) and CNT vibration (red) taken every 6.25 ms. (d) Schematic image of correspondence between a shaken maraca and nanomechanical molecular motion. Adapted with permission from Ref. 40.

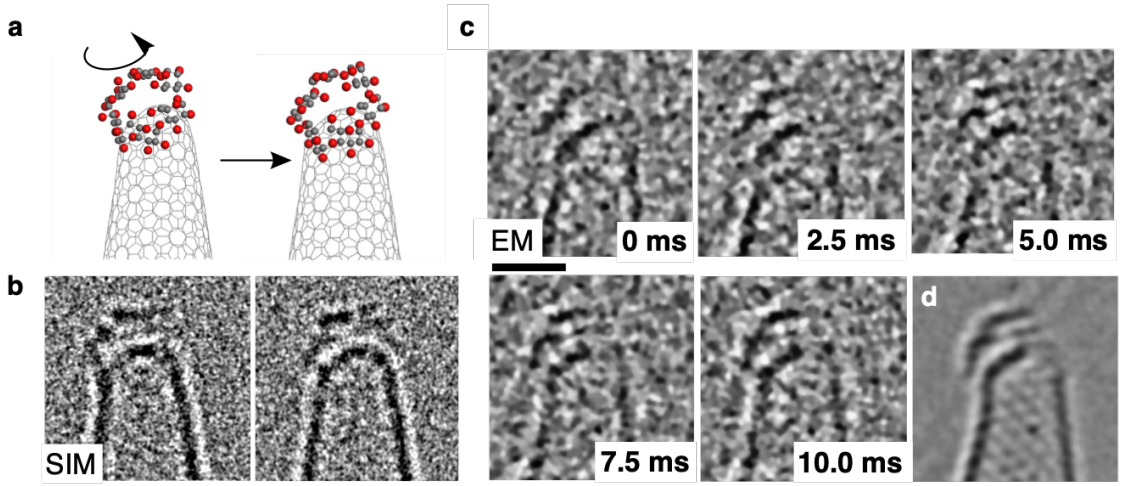

Fig. 7. Dynamics of α-CD (cyclic hexamer of D-glucose) on a conical CNT. (a) Molecular model and (b) simulation of (c) rotation of α-CD taken at 400 fps imaging (scale bar: 1 nm). Changes seen between 0 ms and 2.5 ms, and 7.5 ms and 10.0 ms suggest rotation (and probably conformational change). (d) Superposition of 200 images, equivalent to 2 fps image. Scale bar: 1 nm. Adapted with permission from Ref. 42.

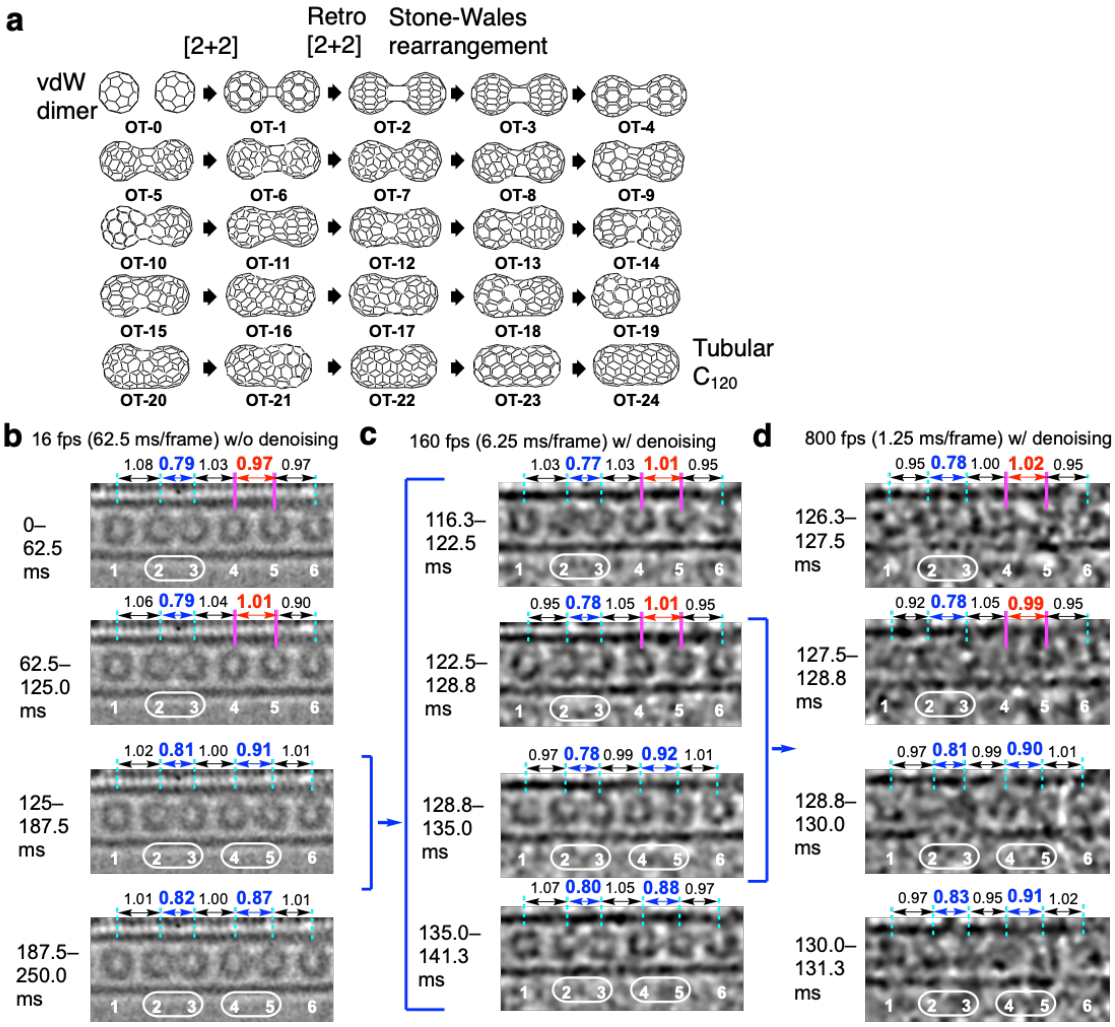

Fig. 8. Cascade reaction and conversion of C_{60} vdW dimer to a dimer recorded at millisecond time resolution. (a) A proposed pathway for converting a C_{60} vdW dimer (**OT-0**) to the short C_{120} nanotube (**OT-24**) through cycloaddition steps and Stone–Wales rearrangements. (b–d) SMART-EM frames showing a cycloaddition event (C_{60} molecules **4** and **5**) in a CNT at 423 K (80 kV, EDR = 2.2 × 10^6 e^- nm^{-2} s^{-1}). C_{60} molecules are numbered below, and dimers are circled together. The numbers above indicate the distance *d* in nm, measured for a stack of frames. (b) Frames of superimposed images without CTV denoising. (c, d) Frames of CTV-denoised and superimposed images with increasing temporal resolution. Adapted with permission from Ref. 52.

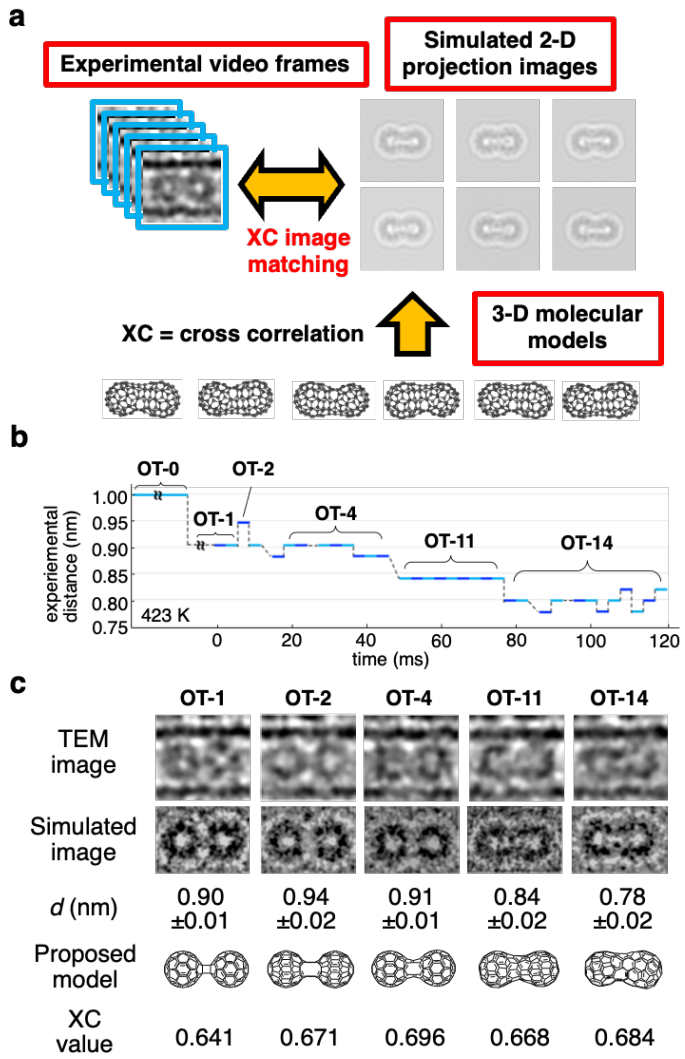

Fig. 9. High-speed deconvolution of the multistep conversion of [2 + 2] cycloadduct **OT-1** to fused dimers. (a) Schematic illustration of structural analysis of a C_{60} dimer determined by XC analysis between experimental TEM images and simulated images generated from candidate intermediate structures. (b) The time evolution of distance *d* was measured every 3.125 ms. To increase the visibility of the figure, each frame is shown alternately in blue and light blue. (c) Experimental and simulated images and *d* of observed intermediates, including the obtained XC values. Adapted with permission from Ref. 52.

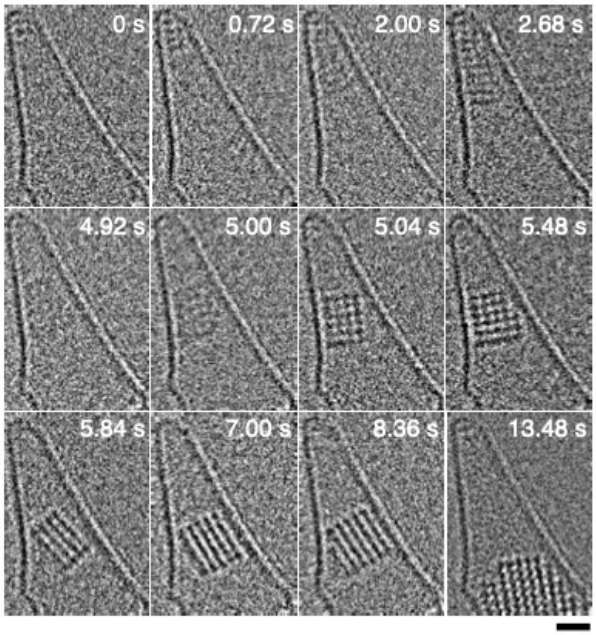

Fig. 10. Images of NaCl crystal nucleation and epitaxial growth in a conical CNT (80 kV, 25 fps, EDR = 4.0×10^5 e^- nm^{-2} s^{-1}). The scale bar is 1 nm. Adapted with permission from Ref. 58.

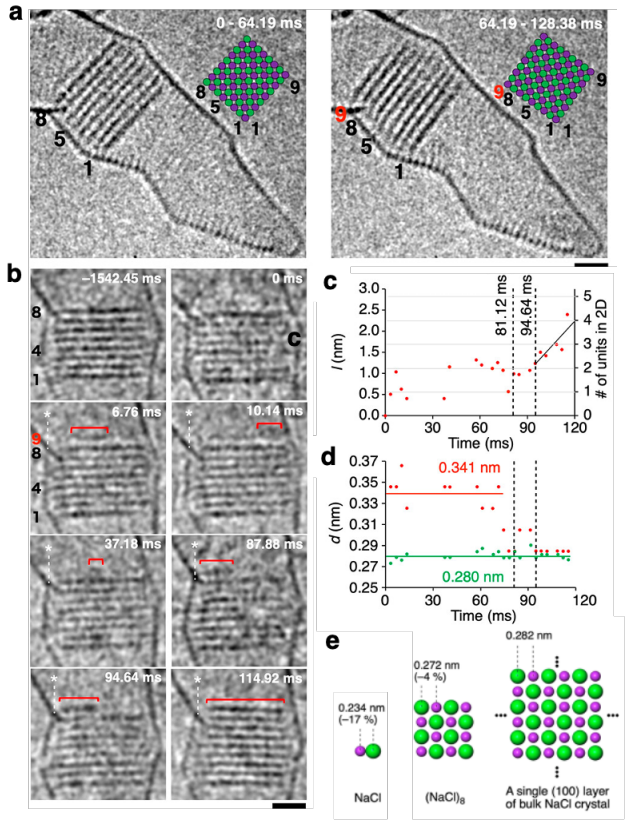

Fig. 11. Observation of migrating FI and lateral growth of terrace of a NaCl nanocrystal (3.38 ms/frame). (a) 20-frame stacked images of the growth of an (8,9) nanocrystal; to a (9,9) nanocrystal. (b) Representative TEM images of NaCl lateral growth. Surface clusters are indicated with red bars. Scale bar: 1 nm. (c) Time evolution of the length of the surface cluster. The black solid line indicates the zeroth-order growth of the terrace size. (d) Time evolution of interlayer distances on the surface cluster (red) and average value on lattice planes (green). Data distribution is because of the 0.020 nm pixel size. (e) Single-layered NaCl clusters exhibit large size-dependency of the Na–Cl distance. The NaCl crystal data show only one layer. Adapted with permission from Ref. 59.

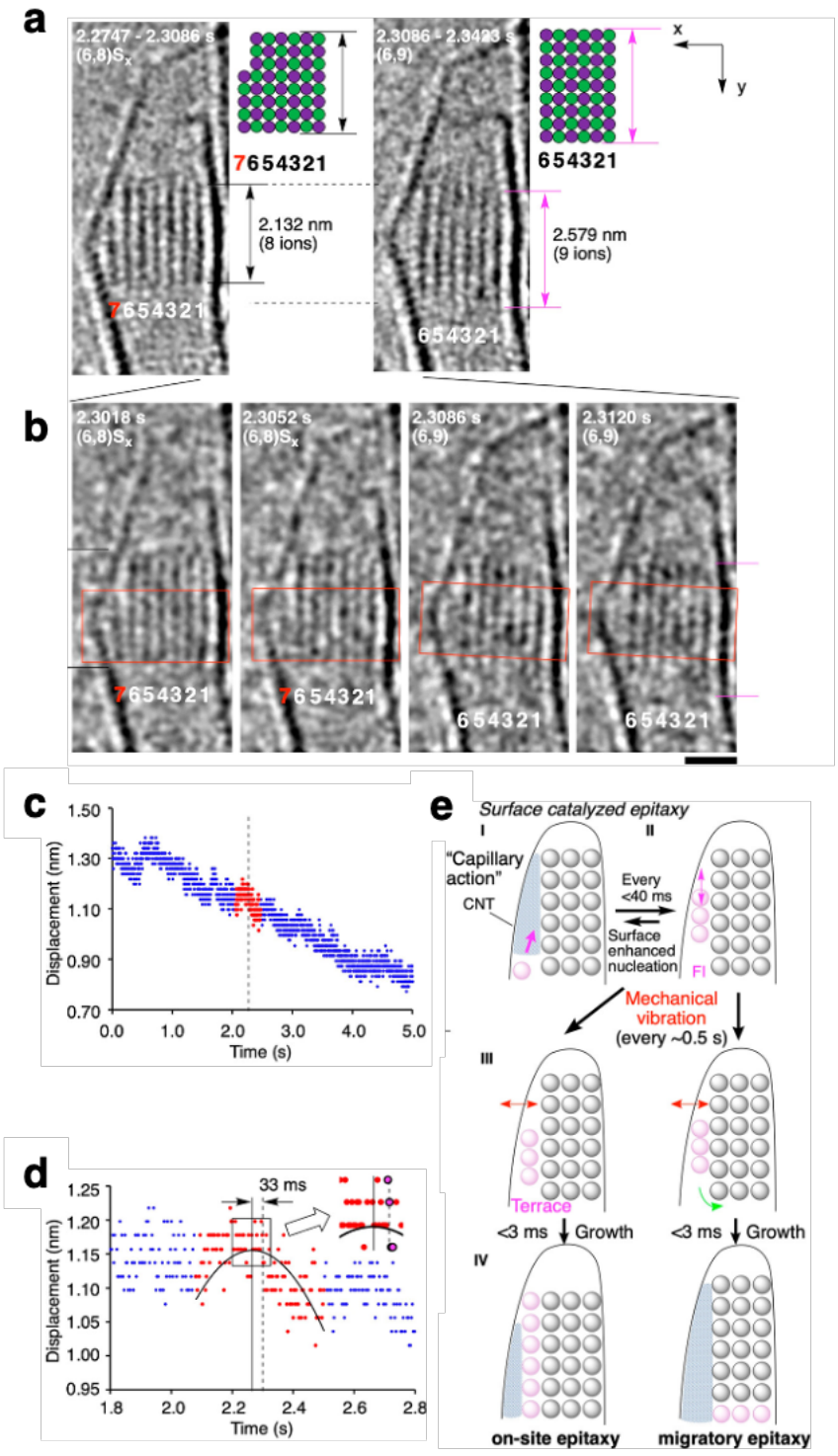

Fig. 12. Observation of migratory epitaxy. (a) 10-frame stacked TEM images of migratory epitaxial growth of a NaCl nanocrystal. (b) Single-shot TEM images with a frame rate of 3.38 ms frame^{-1}. EDR = 2.2 × 10^{6} e^{-} nm^{-2} s^{-1}. Scale bar: 1 nm. (c) A

vibrational plot of the CNT. The persistent decrease in the displacement value is because of the thermal drift of the specimen. The dashed line indicates the frame of crystal growth. (d) Correlation between vibration (quadratic simulation of red dots in black) and FI migration (dashed line). The FI migration occurred at 2.3086 s (dashed line), 33 ms after the CNT vibration was at its maximum amplitude at 2.2750 s (solid line). Inset: purple dots refer to four images in panel b. (e) Schematic illustration of migratory epitaxy in CNT. Red arrows illustrate the vibration of CNT. Migration is shown with a green arrow. Blue mesh presents a low potential space that attracts ion pairs by capillary action. Adapted with permission from Ref. 59.